This paper must be cited as:
Mateos, S. et al. *Small* 2020, DOI: 10.1002/smll.201907171

Instantaneous in vivo imaging of acute myocardial infarct by NIR-II luminescent nanodots

Sergio Mateos[1], Chunyan Li[1,3], Tamara Muñoz-Ortiz[2], Erving C. Ximendes[2,5], María de la Fuente, José Lifante[5], Ángel Luis García Villalón[1], Miriam Granado[1], Jorge Rubio Retama[1,4,5], Daniel Jaque[1, 2,5], Dirk H. Ortgies*[1, 2,5] and Nuria Fernández*[1,5]

[1] Fluorescence Imaging Group, Departamento de Fisiología – Facultad de Medicina, Avda. Arzobispo Morcillo 2, Universidad Autónoma de Madrid, 28029 Madrid, Spain

[2] Fluorescence Imaging Group, Departamento de Física de Materiales – Facultad de Ciencias, Universidad Autónoma de Madrid, C/ Francisco Tomás y Valiente 7, 28049 Madrid, Spain

[3] CAS Key Laboratory of Nano-Bio Interface, Suzhou Key Laboratory of Functional Molecular Imaging Technology, Division of Nanobiomedicine and i-Lab, Suzhou Institute of Nano-Tech and Nano-Bionics, Chinese Academy of Sciences, Suzhou 215123, China, University of Science and Technology of China, Hefei, 230036 China

[4] Departamento de Química Física en Ciencias Farmacéuticas, Facultad de Farmacia, Plaza de Ramón y Cajal, s/n, Universidad Complutense de Madrid, 28040 Madrid, Spain

[5] Nanobiology Group, Instituto Ramón y Cajal de Investigación Sanitaria, IRYCIS, Ctra. Colmenar km. 9.100, 28034 Madrid, Spain

E-mail: nuria.fernandez@uam.es , dirk.ortgies@uam.es

Abstract

Fast and precise localization of ischemic tissues in the myocardium after an acute myocardial infarct is being required by clinicians as the first step towards accurate and efficient treatment. Nowadays, diagnosis of a heart attack at early times is based on biochemical blood analysis (detection of cardiac enzymes) or by ultrasound-assisted imaging. Alternative approaches are investigated to overcome the limitations of these classical techniques (time-consuming procedures or low spatial resolution). As occurs in many other fields of biomedicine, cardiological preclinical imaging can also benefit from the fast development of nanotechnologies. Indeed, bio-functionalized near-infrared-emitting nanoparticles are herein used for in vivo imaging of the heart after an acute myocardial infarct. Taking advantage of the superior acquisition speed of near-infrared fluorescence imaging, and of the efficient selective targeting of our near-infrared-emitting nanoparticles, in vivo images of the infarcted heart were obtained only a few minutes after the acute infarct event. This work opens the avenue towards cost-effective, fast and accurate in vivo imaging of ischemic myocardium tissues after an acute infarct.

1. Introduction

Cardiovascular diseases (CVDs) are responsible for the majority of deaths occurring in the world, especially in low-income and middle-income countries.[1] The increasing impact of CVDs makes it mandatory to improve the diagnostic capabilities of the medical community in order to enable cost-effective diagnosis of a cardiovascular event. Furthermore, fast diagnosis tools of CVDs need to be developed in order to achieve early diagnosis. The efficacy of recovery treatments increases substantially when the consequences of a cardiovascular event (such as an infarct) are known and treated in its early stages. Indeed, early diagnosis provides the extra time required to mitigate the consequences for the patient and without having to place large burdens on health systems.[2,3] Of particular relevance is the early diagnosis,

assessment and treatment of an acute myocardial infarction (heart attack), where an occlusion event in the coronary arteries results in ischemia and lack of oxygen in the myocardium, often causing irreparable damage and/or death.[4] Currently, clinical methods to image and diagnose myocardial infarction rely on low resolution ultrasound imaging, relatively slow biochemical blood analysis, expensive and time-consuming instrumentation (MRI), as well as harmful and expensive nuclear medicine (X-Ray angiography, CAT).[5] The development of a new imaging technique simultaneously capable of cost-effective, fast, and ionizing radiation-free visualization and diagnosis of the heart after an acute infarct remains an unaddressed challenge.[6]

Over the last decade advances made in the synthesis and modification of materials at the nanoscale made the development of novel diagnostic techniques and therapies in biomedicine possible. The increasingly common application of nanomaterials in preclinical settings led to the appearance of a new discipline: nanomedicine. Thanks to the recent development of nanomedicine new and improved techniques for fast diagnosis have been developed, while not over-straining the health budgets of public-health-systems.[7,8] A very promising technique among them is infrared imaging enabled through infrared-emitting luminescent nanoparticles (LNPs) as contrast agent.[9–11] While visible light cannot penetrate biological tissues, photons lying within the so-called near infrared transparency windows can penetrate efficiently into tissues. These windows are spectral region where tissues become partially transparent as their extinction coefficient minimizes. Two biological windows can be defined: 650 – 950 nm (NIR-I) and 1000 – 1700 nm (NIR-II).[12,13] Especially the NIR-II window allows avoiding autofluorescence and presents reduced scattering so that larger penetration depth can be achieved at an improved signal-to-noise ratio.[14,15] The development of LNPs operating in the NIR-II made *in vivo* whole-body imaging in small animals with outstanding resolutions and signal-to-background ratios possible. NIR-II *in vivo* fluorescence imaging has been demonstrated by using rare-earth-doped NPs,[16–19] carbon-based NPs,[20–22] or semiconducting

NPs and quantum dots (QDs).[23–25] In the latter group Ag_2S semiconducting nanodots (NDs) have become quite popular due to their facile synthesis, good brightness, and improved biocompatibility in comparison with the more toxic elements in QDs like Cd or Pb.[26–28] Ag_2S NDs have been successfully employed for in vivo imaging of cancer,[29,30] bloodflow and biodistribution,[31–33] and combined multifunctional / theranostic approaches.[34–36] They also found entry into imaging of cardiovascular diseases.[37,38] Selective targeting of ischemic myocardial tissues is also possible based upon the fact that during a myocardial event the angiotensin receptor 1 (AT1R) of the angiotensin-renin system is overexpressed in the myocardium.[39] The natural ligand for the AT1R is angiotensin II (AngII), which has demonstrated to keep its high binding efficacy also when conjugated to nanoparticles.[40] Dvir et al. explored this functionalization for imaging of heart attacks in mice by employing nano-size PEGylated liposomes conjugated with AngII and loaded with an organic dye (DyLight649). The authors obtained *ex vivo* fluorescence images of infarcted hearts in the NIR-I 24 hours after the infarct and the subsequent injection of luminescent probes.[41] Very recently, AngII-biofunctionalized Ag_2S NDs were successfully employed for NIR-II fluorescence imaging of myocardial infarction in an *ex vivo* Langerdorff model.[42] These results, obtained at the *ex vivo* level, were of importance to demonstrate the suitability of AngII functionalization for imaging of a heart attack but the potential of the technique for NIR-II *in vivo* heart imaging is still left to be demonstrated.

Even though there has been progress in imaging of infarcted heart, it still remains as an unachieved challenge.[10] Previous *in vivo* imaging studies of myocardial infarct were employing either non-optical techniques,[43–46] or sparsely fluorescent nanoparticles working in the visible or in the NIR-I, summarized in **Table 1**[47,48] This made the translation of this research into the clinics difficult, due to the above mentioned drawbacks of visible luminescence imaging (such as poor penetration depth and undesirable overlap with autofluorescence). Furthermore, previous works did not even try to obtain in vivo fluorescent

images of hearts after an acute ischemic event. As can be observed from **Table I,** *in vivo* imaging of infarcted hearts was only obtained on the chronic time-scale. Up to now, *in vivo* images of heart attacks were taken 24 hours after the CVD event, avoiding fast diagnosis after an acute event.

In this work we have employed AngII-functionalized Ag_2S NDs for NIR-II *in vivo* imaging of the heart at short times (minutes) after a myocardial infarct. The analysis of time-course experiments allowed to evaluate the speed of selective targeting of the ischemic myocardial tissues by AngII-functionalized Ag_2S NDs after intravenous injection. A comparison between the bio distribution patterns obtained with the AngII and PEG-functionalized Ag_2S NDs was employed to evaluate the selectivity of our approach.

2. Results and Discussion

Figure 1a illustrates schematically the approach followed in this work. Shortly, the anesthetized mouse is placed in the imaging setup, where illumination with an 808 nm laser diode makes the Ag_2S NDs visible, that have attached to the AT1R in the infarcted heart. The Ag_2S nanoparticles where intravenously injected (100 μl, 1.5 mg mL^{-1}, retroorbital) in a mouse whose left descending coronary artery (LAD) had been ligated previously for 30 min to induce the myocardial infarction (for details see Experimental Section), followed by 30 min reperfusion. This leads to a significant overexpression of the AT1R receptor in the affected myocardial tissue (schematically in **Figure 1a**),[39,41] which results in binding of the injected contrast agent via the AngII on its surface. Excitation at 808 nm with a diode laser at relatively low power densities (0.2 W cm^{-2}) results in a strong NIR-II luminescence emission from the Ag_2S nanoparticles attached to damaged tissues. As we are interested in the fast diagnosis of the infarcted heart, fluorescence images were obtained every 5 minutes during the first hour after intravenous injection of the NIR-II probes. Towards that goal throughout this work two types of LNPs were employed. They were both Ag_2S NDs differentiated by

their surface decoration. For imaging of ischemic myocardium tissues, the Ag_2S nanoparticles were functionalized with AngII (Their Transmission Electron Microscopy (TEM) micrograph is included in **Figure 1b**) and, for non-targeting control experiments we employed PEGylated Ag_2S nanoparticles (for their TEM see Figure S1 in the Supporting Information). Despite the different surface decorations, these two nanoparticles showed very similar hydrodynamic radii, close to 10 nm (see **Figures 1d** and **e**). The two different surface decorations do not produce any relevant change in the emission spectra of the particles, as demonstrated in the literature.[42] The emission spectrum of AngII-functionalized Ag_2S NPs is included in **Figure 1c**. It consist in a highly symmetric broadband centered at 1200 nm that falls well into the NIR-II biological window.

Figure 2a shows the optical, NIR-II fluorescence and merged *in vivo* images of mice as obtained 10 min after the intravenous injection of Ag_2S NDs (40 min after the infarct induction). The NIR-II fluorescence images obtained after performing the heart surgery and injection of Ag_2S-AngII nanoparticles (top row), after surgery and injection of non-targeting PEG-decorated Ag_2S (middle row) and at the bottom after a sham surgery (no infarct) and injection of targeted nanodots are illustrated here. The first row reveals a preferential accumulation of Ag_2S-AngII nanoparticles at the infarcted heart. On the contrary, in absence of an infarct or when using PEGylated Ag_2S NDs, NIR-II fluorescence images clearly demonstrate preferential accumulation in the abdomen due to the retention of nanoparticles in the liver. The NIR-II fluorescence images included in **Figure 2a** demonstrated the successful *in vivo* targeting capability of the employed functionalized Ag_2S-AII and their preferential adhesion to acutely damaged myocardium tissues. Note that after intravenous injection Ag_2S nanoparticles were only preferentially accumulated at the damaged myocardium tissues, when AngII was present as their surface ligand. The two control experiments showed that without targeting or without a myocardial infarct no accumulation in the heart was observed.

In order to evaluate the speed of such preferential targeting of damaged myocardium tissues, time-course experiments were performed. **Figure 2b** shows the time evolution of the NIR-II fluorescence generated at the heart and liver after intravenous injection of Ag_2S-AngII NDs in a mouse subjected to an induced infarct. Data included in **Figure 2b** reveals that the AngII-functionalized nanoparticles accumulate quickly at the infarcted heart. Indeed, accumulation is mainly produced during the first 10 min following intravenous injection. **Figure 2b** also includes the time evolution of the NIR-II fluorescence signal generated by the Ag_2S NDs being accumulated in the liver. Note that, contrary to what is observed at the heart, the NIR-II fluorescence signal generated from the liver decreases monotonously with time, indicating an initial retention by the liver likely followed by a gradual release either through the bile (feces) and/or through the kidneys (urine) of Ag_2S NDs. **Figure 2c** shows the time evolution of the NIR-II fluorescence intensity generated by PEGylated Ag_2S NDs accumulated at both the heart and liver after intravenous injection into a mouse subjected to an acute infarct. In this case, the time evolution of the NIR-II intensity generated at both organs follow a completely different pattern. In this case, preferential retention at the liver is observed, even for the very short times. Note that after intravenous injection, the NIR-II intensity generated at the liver remains virtually constant. This indicates a preferential accumulation in the liver of PEGylated Ag_2S NDs. Time profiles included in **Figure 2c** clearly indicate a long-term retention of PEGylated Ag_2S NDs at the liver. At the same time, no significant preferential accumulation at the heart is observed. At short times after injection, PEGylated Ag_2S NDs are present at the heart, due to their permanence in the circulatory system. Nevertheless, the NIR-II fluorescence generated by the PEGylated Ag_2S NDs at the heart decreases monotonously with time. The time decay can be fitted to an exponential decay curve, revealing a characteristic circulation time of PEGylated Ag_2S NDs in the bloodstream close to 20 min. The time profiles included in **Figures 2b and c** do not only reveal the suitability of AngII-decorated Ag_2S NDs for selective targeting of the damaged myocardium after the acute heart

attack, but also reveal their capability for fast diagnosis as selective accumulation is produced on a short time scale: 10 min after the injection are sufficient time to observe a clear and specific signal from ischemic myocardial tissues.

In order to obtain evidence that the *in vivo* NIR-II fluorescence signal detected from myocardium in **Figure 2a** is unequivocally correlated with the presence of Ag_2S NDs, the animals were sacrificed 1 hour after the NPs injection. The hearts were immediately dissected and analyzed via NIR-II hyperspectral imaging. A detailed description of the experimental system used for NIR-II hyperspectral imaging can be found in **Experimental Section**. **Figure 3a** shows luminescence images obtained at 1000, 1200 and 1500 nm of explanted hearts corresponding to the three situations studied in this work. The top row illustrates the case of an infarcted heart after intravenous injection of AngII Ag_2S NDs (Infarcted+AngII-Ag_2S case). No luminescence neither at 1000 nor at 1500 nm was observed. The fluorescence image obtained at 1200 nm shows a clear signal generated at the top of the heart, where the most relevant damage of myocardial tissue has been produced. The fact that fluorescence image is detected at 1200 nm suggest that the luminescence contrast is being provided by the AngII Ag_2S NDs. The emission spectra obtained from the analysis of the hyperspectral cube as obtained in the top area of the heart is included in **Figure 3b**. It well matches the emission spectra of Ag_2S NDs in a colloidal suspension (see **Figure 1c**), clearly indicating that the observed luminescence can be attributed to the selective attachment of AngII Ag_2S NDs to the ischemic myocardium tissues. The middle row in **Figure 3a** shows the NIR-II luminescence images obtained from a healthy heart after intravenous injection of AngII Ag_2S NDs (Healthy+AngII-Ag_2S case). Again, no signal is observed at 1000 and 1500 nm and the fluorescence image obtained at 1200 nm is barely above the background. The emission spectra obtained for this healthy control heart is also included in **Figure 3b**. The obtained spectrum does not closely resemble the emission spectrum of Ag_2S nanodots, indicating negligible accumulation in the healthy heart and the necessity of an ischemic event in order to

increase AT1R expression and accumulation. Finally, the bottom row in **Figure 3a** shows the fluorescence images at the three analyzed wavelengths of an infarcted heart after intravenous injection of PEGylated Ag_2S NDs (Infarcted+PEG-Ag_2S case). In this case, only a very weak signal is observed at 1200 nm. This suggest a minimal accumulation if any at all of NDs. Data included in **Figure 3b** reveals that the emission spectra obtained in this case is broadband centered at 1200 nm although weaker than for AngII-Ag_2S NDs. This can be correlated with a small presence of PEGylated Ag_2S NDs in the ischemic myocardium tissues probably due to the enhanced permeability and retention effect (EPR), which can occur in ischemic myocardial tissues.[45,49] Triphenyl tetrazolium chloride (TTC) staining further corroborated these findings as shown in **Figure S3** in the Supporting Information, confirming the control heart (sham operation, healthy heart case) did not show damages and was in fact a healthy heart (**Figure S3a**) while the infarcted heart with damaged tissue principally in the tip, which had been exposed to AngII-Ag2S nanodots, is shown in **Figure S3b**. A collateral question rising at this point is the origin of the fluorescence observed in the spectra in **Figure 3** (likely autofluorescence) generated by the heart in absence of Ag_2S NDs. This question is out of the scope of this work and will deserve detailed investigation in the near future. Nevertheless, we state at this point that this emission band very likely corresponds to the NIR-II autofluorescence of heart.

In order to further analyze the presence of an infarct and the overexpression of AT1R, a reverse transcriptase qualitative polymerase chain reaction (qt-PCR) was performed with samples obtained from the infarcted hearts. **Figure 3c** shows the percentage of AT1R expression as obtained for the three cases (healthy heart, infarcted heart: undamaged tissue and infarcted heart: damaged tissues) based on the mRNA expression levels that were analyzed as described in the **Experimental Section**. As expected, the healthy heart shows the lowest expression of AT1R, while it is slightly elevated in the healthy areas of an infarcted heart and substantially elevated in the damaged myocardial tissues. Data included in **Figure**

3c can now be correlated with the integrated intensity of the three emission spectra included in **Figure 3b** and that are included in **Figure 3d**. This graph effectively visualizes the targeting efficiency of our AngII-functionalized Ag_2S NDs for the detection of ischemic myocardium tissues. It also allows to quantify it. Note that the infarct induction leads to a relative increment in the ATR1 expression of less than 50% in **Figure 3c** whereas the NIR-II fluorescence signal associated to the selective accumulation of Ag_2S AngII NDs shows a 10-fold increment. This, again, reveals a highly efficient targeting at short circulation times. Finally, the AT1R-targeting capabilities of our AngII-functionalized Ag_2S NDs were further investigated by the acquisition of biodistribution patterns. Towards this goal, the NIR-II luminescence images of exerted organs from the three cases studied in **Figure 3** were systematically acquired. **Figure 4a** shows that PEGylated Ag_2S NDs accumulate preferentially in the liver and spleen, while all other organs did not show any infrared luminescence, as was the case for the control experiment without an infarct, which also resulted in accumulation in liver and spleen. In contrast, in the organs from the mouse injected with AngII-functionalized Ag_2S NDs after the infarct induction, luminescence is only present in the heart and in the lungs. This is in good agreement with the data included in **Figure 2b**, revealing a negligible retention of these Ag_2S NDs by liver or spleen. The accumulation at the lungs of the AngII-functionalized Ag_2S NDs was initially surprising but it could be explained due to a dysfunction of the alveolar-capillary barrier that may lead to pulmonary congestion,[50,51] which would cause the extravasation of the non-targeted NPs.[52] Moreover, mechanical ventilation may cause ventilator-induced lung injury (VILI) even when the least injurious ventilator settings are used.[53] In the pathogenesis of VILI inflammation plays an important role, and upregulation of lung angiotensin receptors could be present as part of inflammatory response.[54]

3. Conclusion

This work demonstrates that fast and highly selective in vivo heart imaging after an acute infarct is, indeed, possible by using NIR-II emitting Ag_2S nanodots functionalized with the peptide angiotensin II. Results include in this work demonstrate how the efficient overexpression of the AT1R receptor after an acute infarct enables the instantaneous (< 10 min) and selective targeting of intravenously injected AngII-functionalized Ag_2S nanodots to ischemic myocardial tissues. The strong luminescence of Ag_2S nanodots in the second infrared transparency window makes the real time in vivo visualization hearts damaged by an acute infarct possible by the earliest time. Comparison of the hyperspectral images of ex-vivo organs has been employed to reinforce the high specificity of AngII-functionalized Ag_2S nanodots to attach to ischemic myocardium tissues even during systemic injection.

This work introduces to the scientific community NIR-II emitting nanoparticles for fast in vivo imaging and diagnosis of hearts after an acute infarct. This constitutes a first step towards early and speedy diagnosis at the pre-clinical level of myocardial infarct and, therefore, could contribute to the development of new therapy routes. In addition, the high targeting ability of AngII-functionalized Ag_2S to detect and localize ischemic myocardium tissues also opens the door to new therapy approaches based on drug delivery or in the ability of Ag_2S nanodots to produce simultaneous local hyperthermia and contactless thermal sensing.

4. Experimental Section

Ag_2S nanodots: Ag_2S-AngII were obtained from SINANO Int (China) at a concentration of 1.5 mg mL^{-1} in PBS. Ag_2S-AngII is coated with polyethyleneglycol and further modified via the carboxy terminus of the PEG with angiotensin II and 4 Glycine residues as spacer (Gly-Gly-Gly-Gly-Asp-Arg-Val-Tyr-Ile-His-Pro-Phe). The Ag_2S-PEG non-targeted nanoparticles were synthesized and characterized as given in previous publications.[28] Shortly, silver diethyldithiocarbamate AgDDTC (0.1 mmol) was dispersed in dodecanethiol (5 mL). The

mixture was submitted to vacuum for 10 min to remove air and then filled with N_2. After that, the mixture was heated to 190 ºC with a heating rate of 20 ºC min^{-1} and under slow magnetic stirring. The temperature was kept for 1 hour and later cooled down to room temperature naturally. The synthesized nanoparticles were collected by addition of absolute ethanol (10 mL), reducing the colloidal stability of the LNPs for collection via centrifugation (10,000 rpm for 10 min). This process was repeated twice. The as-prepared product was re-dispersed in chloroform (10 mL) and stored for further steps. With the aim of providing hydrophilicity to the synthesized LNPs, they were treated with 11-mercaptoundecanoic acid (MUA). This molecule introduced carboxylic groups on the surface of the nanoparticles, which provided colloidal stability in water. With that purpose, MUA (20 mg, 0.1 mmol) of MUA was added to a dispersion of Ag_2S nanoparticles in chloroform (1 mL, 1 mg mL^{-1}). After that, the mixture was sonicated in an ultrasonic bath for 10 minutes until the Ag_2S nanoparticles lost their colloidal stability and precipitated in the bottom of the flask. The precipitate was collected and dispersed in PBS (1 mL) at pH 7.4. The resulting nanoparticles exhibit a Z-potential of –34 mV due to the presence the negatively charged carboxylate groups on the surface of the nanoparticles. Subsequently these nanoparticles were covered with PEG (Mw=2500 g/mol) via EDC/NHS coupling. EDC (0.5 mg) and sulfo-NHS (0.7 mg) were dissolved in PBS (1 mL) containing the previously prepared Ag_2S NDs (1 mg) and mPEG-NH_2 (1 mg). The mixture was gently stirred for 2 hours and after this time the nanoparticles were collected by centrifugation at 12.000 rpm for 4 hours. This process was repeated three times and the resulting nanoparticles were dispersed in PBS (1 mL) and stored at 4 ºC. The Z-potential of these nanoparticles is reduced to –17 mV, as a result of the transformation of part of the carboxylate groups into amide bonds.

Morphological characterization: Transmission electron microscopy was performed on a JEOL JEM 1010 microscope operating at 80 kV. The carbon coated copper TEM grid was loaded with sample by placing one drop of a dilute aqueous dispersion onto it and letting it

dry for 10 min. The size distributions were obtained through analysis via ImageJ of ensembles of over 200 particles in randomly selected areas of the enlarged micrographs.

Animal Studies: 15 CD1 2 month old male and female mice were employed in this study. All animal experiments were approved by the Animal Ethics Committee of the Universidad Autónoma de Madrid and conducted in accordance with the European Union directive 63/2010UE and the Spanish regulation RD 53/2013. The acute myocardial ischemia-reperfusion injury was performed through ligation of the Left Anterior Descending Artery (LAD) following the protocol described by Xu et al.[55] Sedation of the animal was achieved through a combination of Xylazine (0.2 mL) and Ketamine (0.3 mL) mixed with saline solution (0.15 mL) and administrating 0.15 ml of anesthetic per 30 g of animal body weight, via intraperitoneal injection. Prior to the intervention, the chest and the left side of the intercostal area of the animal were shaved and cleaned with 95% alcohol. Afterwards, orotracheal intubation was performed. For the orotracheal intubation of the animal, we exposed the trachea by a median cervical skin incision with the animal in a supine position and separated the lobes of the thyroidal gland and the muscle below, exposing the trachea. This allowed the introduction of an intubation tube (Insyte-W, 0.9 x 25 mm) with the help of a needle, which had the tip cut to prevent damage, confirming the correct position inside the trachea with a magnifying glass. After a correct orotracheal intubation, a constant flow of 0.8% isoflurane anesthetic in 100% oxygen with a flow rate of 170 breaths/minute and an external positive end-expiratory airway pressure (PEEP) from 2-10 cm_{H2O} was maintained an external small animal ventilator (VentElite 55-7040, Harvard Apparatus). To maintain the temperature of the animal, the procedure was performed on a heating pad and the animal temperature was controlled with a rectal probe. In order to gain access to the heart, the intercostal space between the 3rd and 4th ribs was opened, the pericardium was removed and the LAD was identified below the left auricle. The ligation was performed before the bifurcation of the LAD with an 8-0 silk suture. Between the LAD and silk suture, before

closing the knot, a plastic tube of 2-3 mm was placed in order to be able to reperfusion. The ligation of the LAD was performed for 30 minutes until reperfusion, which was maintained for another 30 min and after that, we moved the mouse to the imaging setup and injected the NPs to study their biodistribution.

Quantification of AT-1 gene expression in myocardial tissue by RT-qPCR: Total RNA was extracted from 100mg of myocardiac tissue using the Trizol method and quantified with a Nanodrop2000 spectrometer (Thermo Fisher Scientific, Hampton, NH, EE.UU).[56] Afterwards, 1µg of total RNA was retrotranscribed into cDNA using a high capacity cDNA reverse transcription kit (Applied Biosystems, Foster City, CA, USA). The mRNA levels of AT-1 were measured by quantitative real-rime PCR. The assay was performed by using an on-demand assay probe (Applied Biosystems, Foster City, CA, USA,) for this specific gene (Mm_ 00616371_m1). TaqMan Universal PCR Master Mix (Applied Biosystems, Foster City, CA, USA) was used for amplification in a Step One thermocycler (Applied Biosystems, Foster City, CA, USA). To determine relative expression levels the ΔCT method was used.[57] Values were normalized to the housekeeping gene 18S.

Infrared fluorescence Imaging: The anesthetized and operated animals were located in the field of view of an InGaAs camera (Xeva1.7-320) with high sensitivity in the IR spectral range (1000 – 1700 nm). Excitation was performed by a fiber-coupled 808 nm laser diode (LIMO) placed next to the camera objective in order to create a spot of 35 cm^2, resulting in an illumination of 0.2 W/cm^2. The 808 nm scattering background of the laser diode was eliminated by 2 long pass filter with a cutoff wavelengths of 850 nm (Thorlabs FEL850) and 1050 nm (Thorlabs FEL1050) between the objective and the camera.

Hyperspectral Imaging: The freshly dissected heart was excited with the same continuous laser (LIMO) via a fiber of 808 placed next to the camera objective and power and distance were regulated to achieve an illumination intensity of 50 mW/cm2. An exposure time of 20 s and a spatial resolution of 10 nm was selected for all hyperspectral imaging studies. A short-

pass filter (Thorlabs FES0850) was placed immediately in front of the laser fiber to minimize specular and diffuse reflection effects. The scattered light emitted from the sample was transmitted through two consecutive long-pass filter (Thorlabs FL0850) that were intended to suppress signal from the laser. Tube and shortwave infrared (SWIR) lenses were used as a relay to build up the fluorescence image on a Bragg tunable filter which allows to select a specific wavelength of the incoming light. A second tube lens focuses after the filtered light on an infrared camera (ZephIRTM 1.7) to produce a monochromatic image, while the non-filtered light follows a different optical path. To cover a specific spectral range, each monochromatic image needed to be acquired and then stored on a computer while the angle of the BTF rotation stage is set to the next wavelength. After n steps, one would then have what is called a HSI cube, i.e. a 3D spatial map of spectral variation: the first two dimensions providing spatial information and a third dimension accounting for the spectral information. The intensity values of a particular pixel in a HIS cube characterize its unique spectral fingerprint.[58]

Spectroscopic Characterization: The emission spectra were obtained upon excitation with a fiber-coupled 790 nm laser diode (Lumics) focused in a quartz cuvette filled with the aqueous dispersion of Ag_2S nanodots (concentration 1.5 mg mL^{-1}). The luminescence signal was collected by an InGaAs camera (Andor iDus DU490A) after passing through appropriate filters and being spectrally analyzed by an Andor Shamrock 193i spectrometer.

Supporting Information

Supporting Information providing additional characterization data (TEM, FTIR, staining) is available from the Wiley Online Library or from the author.

Acknowledgements

Support by the Ministerio de Economía y Competitividad de España (MAT2016-75362-C3-1-R) and (MAT2017-83111R), by the Instituto de Salud Carlos III (PI16/00812), by the Comunidad Autónoma de Madrid (B2017/BMD-3867RENIMCM), co-financed by the European Structural and investment funds, is acknowledged. Additionally, the investigation was supported by the European Commission Horizon 2020 project NanoTBTech, the Fundación para la Investigación Biomédica del Hospital Universitario Ramón y Cajal project

IMP18_38 (2018/0265), and also by COST action CM1403. D. H. O. is grateful to the Instituto de Salud Carlos III for a Sara Borrell scholarship (No. CD17/00210). The authors are grateful to David Sabador Osuna for preparing Figure 1a.

Received: ((will be filled in by the editorial staff))
Revised: ((will be filled in by the editorial staff))
Published online: ((will be filled in by the editorial staff))

References

[1] S. Kaptoge, L. Pennells, D. De Bacquer, M. T. Cooney, M. Kavousi, G. Stevens, L. M. Riley, S. Savin, T. Khan, S. Altay, P. Amouyel, G. Assmann, S. Bell, Y. Ben-Shlomo, L. Berkman, J. W. Beulens, C. Björkelund, M. Blaha, D. G. Blazer, T. Bolton, R. Bonita Beaglehole, H. Brenner, E. J. Brunner, E. Casiglia, P. Chamnan, Y.-H. Choi, R. Chowdry, S. Coady, C. J. Crespo, M. Cushman, G. R. Dagenais, R. B. D'Agostino Sr, M. Daimon, K. W. Davidson, G. Engström, I. Ford, J. Gallacher, R. T. Gansevoort, T. A. Gaziano, S. Giampaoli, G. Grandits, S. Grimsgaard, D. E. Grobbee, V. Gudnason, Q. Guo, H. Tolonen, S. Humphries, H. Iso, J. W. Jukema, J. Kauhanen, A. P. Kengne, D. Khalili, W. Koenig, D. Kromhout, H. Krumholz, T. Lam, G. Laughlin, A. Marín Ibañez, T. W. Meade, K. G. M. Moons, P. J. Nietert, T. Ninomiya, B. G. Nordestgaard, C. O'Donnell, L. Palmieri, A. Patel, P. Perel, J. F. Price, R. Providencia, P. M. Ridker, B. Rodriguez, A. Rosengren, R. Roussel, M. Sakurai, V. Salomaa, S. Sato, B. Schöttker, N. Shara, J. E. Shaw, H.-C. Shin, L. A. Simons, E. Sofianopoulou, J. Sundström, H. Völzke, R. B. Wallace, N. J. Wareham, P. Willeit, D. Wood, A. Wood, D. Zhao, M. Woodward, G. Danaei, G. Roth, S. Mendis, O. Onuma, C. Varghese, M. Ezzati, I. Graham, R. Jackson, J. Danesh, E. Di Angelantonio, *Lancet Glob. Heal.* **2019**, *7*, e1332.

[2] M. Mahmoudi, M. Yu, V. Serpooshan, J. C. Wu, R. Langer, R. T. Lee, J. M. Karp, O. C. Farokhzad, *Nat. Nanotechnol.* **2017**, *12*, 845.

[3] F. Sanchis-Gomar, C. Perez-Quilis, R. Leischik, A. Lucia, *Ann. Transl. Med.* **2016**, *4*,

1.

[4] E. Ruvinov, T. Dvir, J. Leor, S. Cohen, *Expert Rev. Cardiovasc. Ther.* **2008**, *6*, 669.

[5] F. A. Flachskampf, M. Schmid, C. Rost, S. Achenbach, A. N. DeMaria, W. G. Daniel, *Eur. Heart J.* **2011**, *32*, 272.

[6] C. M. Kramer, A. J. Sinusas, D. E. Sosnovik, B. A. French, F. M. Bengel, *J. Nucl. Med.* **2010**, *51*, 107S.

[7] O. Lozano, A. Torres-Quintanilla, G. García-Rivas, *J. Control. Release* **2018**, *271*, 149.

[8] J. Bejarano, M. Navarro-Marquez, F. Morales-Zavala, J. O. Morales, I. Garcia-Carvajal, E. Araya-Fuentes, Y. Flores, H. E. Verdejo, P. F. Castro, S. Lavandero, M. J. Kogan, *Theranostics* **2018**, *8*, 4710.

[9] G. Hong, A. L. Antaris, H. Dai, *Nat. Biomed. Eng.* **2017**, *1*, 0010.

[10] J. Hu, D. H. Ortgies, E. Martín Rodríguez, F. Rivero, R. Aguilar Torres, F. Alfonso, N. Fernández, G. Carreño-Tarragona, L. Monge, F. Sanz-Rodriguez, M. del C. Iglesias, M. Granado, A. L. García-Villalon, J. García Solé, D. Jaque, *Adv. Opt. Mater.* **2018**, *6*, 1800626.

[11] D. Jaque, C. Richard, B. Viana, K. Soga, X. Liu, J. García Solé, *Adv. Opt. Photonics* **2016**, *8*, 1.

[12] A. M. Smith, M. C. Mancini, S. Nie, *Nat. Nanotechnol.* **2009**, *4*, 710.

[13] E. Hemmer, A. Benayas, F. Légaré, F. Vetrone, *Nanoscale Horizons* **2016**, *1*, 168.

[14] B. del Rosal, I. Villa, D. Jaque, F. Sanz-Rodríguez, *J. Biophotonics* **2016**, *9*, 1059.

[15] B. del Rosal, A. Benayas, *Small Methods* **2018**, *2*, 1800075.

[16] L. Labrador-Páez, E. C. Ximendes, P. Rodríguez-Sevilla, D. H. Ortgies, U. Rocha, C. Jacinto, E. Martín Rodríguez, P. Haro-González, D. Jaque, *Nanoscale* **2018**, *10*, 12935.

[17] Y. Liu, D. Tu, H. Zhu, X. Chen, *Chem. Soc. Rev.* **2013**, *42*, 6924.

[18] B. Liu, C. Li, P. Yang, Z. Hou, J. Lin, *Adv. Mater.* **2017**, *29*, 1605434.

[19] I. Villa, A. Vedda, I. X. Cantarelli, M. Pedroni, F. Piccinelli, M. Bettinelli, A.

Speghini, M. Quintanilla, F. Vetrone, U. Rocha, C. Jacinto, E. Carrasco, F. S. Rodríguez, Á. Juarranz, B. del Rosal, D. H. Ortgies, P. H. Gonzalez, J. G. Solé, D. J. García, *Nano Res.* **2015**, *8*.

[20] K. Welsher, S. P. Sherlock, H. Dai, *Proc. Natl. Acad. Sci.* **2011**, *108*, 8943.

[21] J. T. Robinson, G. Hong, Y. Liang, B. Zhang, O. K. Yaghi, H. Dai, *J. Am. Chem. Soc.* **2012**, *134*, 10664.

[22] R. Bhavane, Z. Starosolski, I. Stupin, K. B. Ghaghada, A. Annapragada, *Sci. Rep.* **2018**, *8*, 14455.

[23] A. Benayas, F. Ren, E. Carrasco, V. Marzal, B. del Rosal, B. A. Gonfa, Á. Juarranz, F. Sanz-Rodríguez, D. Jaque, J. García-Solé, D. Ma, F. Vetrone, *Adv. Funct. Mater.* **2015**, *25*, 6650.

[24] Y. Imamura, S. Yamada, S. Tsuboi, Y. Nakane, Y. Tsukasaki, A. Komatsuzaki, T. Jin, *Molecules* **2016**, *21*.

[25] S. Jeong, Y. Jung, S. Bok, Y.-M. Ryu, S. Lee, Y.-E. Kim, J. Song, M. Kim, S.-Y. Kim, G.-O. Ahn, S. Kim, *Adv. Healthc. Mater.* **2018**, *7*, 1800695.

[26] S. I. Sadovnikov, A. I. Gusev, *J. Mater. Chem. A* **2017**, *5*, 17676.

[27] Y. Zhang, G. Hong, Y. Zhang, G. Chen, F. Li, H. Dai, Q. Wang, *ACS Nano* **2012**, *6*, 3695.

[28] G. Hong, J. T. Robinson, Y. Zhang, S. Diao, A. L. Antaris, Q. Wang, H. Dai, *Angew. Chem. Int. Ed.* **2012**, *51*, 9818.

[29] F. Hu, C. Li, Y. Zhang, M. Wang, D. Wu, Q. Wang, *Nano Res.* **2015**, *8*, 1637.

[30] H. D. A. Santos, E. C. Ximendes, M. del C. Iglesias-de la Cruz, I. Chaves-Coira, B. del Rosal, C. Jacinto, L. Monge, I. Rubia-Rodríguez, D. Ortega, S. Mateos, J. GarcíaSolé, D. Jaque, N. Fernández, *Adv. Funct. Mater.* **2018**, *28*, 1803924.

[31] C. Li, F. Li, Y. Zhang, W. Zhang, X. E. Zhang, Q. Wang, *ACS Nano* **2015**, *9*, 12255.

[32] Y. Zhang, Y. Zhang, G. Hong, W. He, K. Zhou, K. Yang, F. Li, G. Chen, Z. Liu, H.

Dai, Q. Wang, *Biomaterials* **2013**, *34*, 3639.

[33] C. Li, Y. Zhang, M. Wang, Y. Zhang, G. Chen, L. Li, D. Wu, Q. Wang, *Biomaterials* **2014**, *35*, 393.

[34] C. Lu, G. Chen, B. Yu, H. Cong, *Adv. Eng. Mater.* **2018**, *20*, 1700940.

[35] Y. Shen, J. Lifante, E. Ximendes, H. D. A. Santos, D. Ruiz, B. H. Juárez, I. Zabala Gutiérrez, V. Torres Vera, J. Rubio Retama, E. Martín Rodríguez, D. H. Ortgies, D. Jaque, A. Benayas, B. del Rosal, *Nanoscale* **2019**.

[36] T. Yang, Y. Tang, L. Liu, X. Lv, Q. Wang, H. Ke, Y. Deng, H. Yang, X. Yang, G. Liu, Y. Zhao, H. Chen, *ACS Nano* **2017**, *11*, 1848.

[37] C. Wu, Y. Zhang, Z. Li, C. Li, Q. Wang, *Nanoscale* **2016**, *8*, 12531.

[38] G. Hong, J. C. Lee, A. Jha, S. Diao, K. H. Nakayama, L. Hou, T. C. Doyle, J. T. Robinson, A. L. Antaris, H. Dai, J. P. Cooke, N. F. Huang, *Circ. Cardiovasc. Imaging* **2014**, *7*, 517.

[39] B. Molavi, J. Chen, J. L. Mehta, *Am. J. Physiol. Circ. Physiol.* **2006**, *291*, H687.

[40] R. Hennig, K. Pollinger, J. Tessmar, A. Goepferich, *J. Drug Target.* **2015**, *23*, 681.

[41] T. Dvir, M. Bauer, A. Schroeder, J. H. Tsui, D. G. Anderson, R. Langer, R. Liao, D. S. Kohane, *Nano Lett.* **2011**, *11*, 4411.

[42] D. H. Ortgies, Á. L. García-Villalón, M. Granado, S. Amor, E. M. Rodríguez, H. D. A. Santos, J. Yao, J. Rubio-Retama, D. Jaque, *Nano Res.* **2019**, *12*, 749.

[43] D. E. Sosnovik, E. A. Schellenberger, M. Nahrendorf, M. S. Novikov, T. Matsui, G. Dai, F. Reynolds, L. Grazette, A. Rosenzweig, R. Weissleder, L. Josephson, *Magn. Reson. Med.* **2005**, *54*, 718.

[44] D. E. Sosnovik, E. Garanger, E. Aikawa, M. Nahrendorf, L. Jose-Figuiredo, G. Dai, F. Reynolds, A. Rosenzweig, R. Weissleder, L. Josephson, *Circ. Cardiovasc. Imaging* **2009**, *2*, 460.

[45] M. J. Lipinski, M. T. Albelda, J. C. Frias, S. A. Anderson, D. Luger, P. C. Westman, R.

O. Escarcega, D. G. Hellinga, R. Waksman, A. E. Arai, S. E. Epstein, *Cardiovasc. Revascularization Med.* **2016**, *17*, 106.

[46] M. P. A. Ferreira, S. Ranjan, S. Kinnunen, A. Correia, V. Talman, E. Mäkilä, B. Barrios-Lopez, M. Kemell, V. Balasubramanian, J. Salonen, J. Hirvonen, H. Ruskoaho, A. J. Airaksinen, H. A. Santos, *Small* **2017**, *13*, 1.

[47] D. E. Sosnovik, M. Nahrendorf, N. Deliolanis, M. Novikov, E. Aikawa, L. Josephson, A. Rosenzweig, R. Weissleder, V. Ntziachristos, *Circulation* **2007**, *115*, 1384.

[48] M. Nahrendorf, D. E. Sosnovik, P. Waterman, F. K. Swirski, A. N. Pande, E. Aikawa, J. L. Figueiredo, M. J. Pittet, R. Weissleder, *Circ. Res.* **2007**, *100*, 1218.

[49] D. J. Lundy, K. H. Chen, E. K. W. Toh, P. C. H. Hsieh, *Sci. Rep.* **2016**, *6*, 1.

[50] L. Pappas, G. Filippatos, *Rev. Española Cardiol. (English Ed.* **2011**, *64*, 735.

[51] L. Pavone, S. Albert, J. DiRocco, L. Gatto, G. Nieman, *Crit. Care* **2007**, *11*, R104.

[52] J. C. Grimm, F. Zhang, J. T. Magruder, T. C. Crawford, M. Mishra, K. M. Rangaramanujam, A. S. Shah, *J. Surg. Res.* **2017**, *210*, 78.

[53] E. K. Wolthuis, A. P. Vlaar, G. Choi, J. J. Roelofs, N. P. Juffermans, M. J. Schultz, *Crit. Care* **2009**, *13*, R1.

[54] J.-S. Jerng, Y.-C. Hsu, H.-D. Wu, H.-Z. Pan, H.-C. Wang, C.-T. Shun, C.-J. Yu, P.-C. Yang, *Thorax* **2007**, *62*, 527.

[55] Z. Xu, J. Alloush, E. Beck, N. Weisleder, *J. Vis. Exp.* **2014**.

[56] P. Chomzynski, *Anal. Biochem.* **1987**, *162*, 156.

[57] K. J. Livak, T. D. Schmittgen, *Methods* **2001**, *25*, 402.

[58] S. Zhu, S. Herraiz, J. Yue, M. Zhang, H. Wan, Q. Yang, Z. Ma, Y. Wang, J. He, A. L. Antaris, Y. Zhong, S. Diao, Y. Feng, Y. Zhou, K. Yu, G. Hong, Y. Liang, A. J. Hsueh, H. Dai, *Adv. Mater.* **2018**, *30*, 1705799.

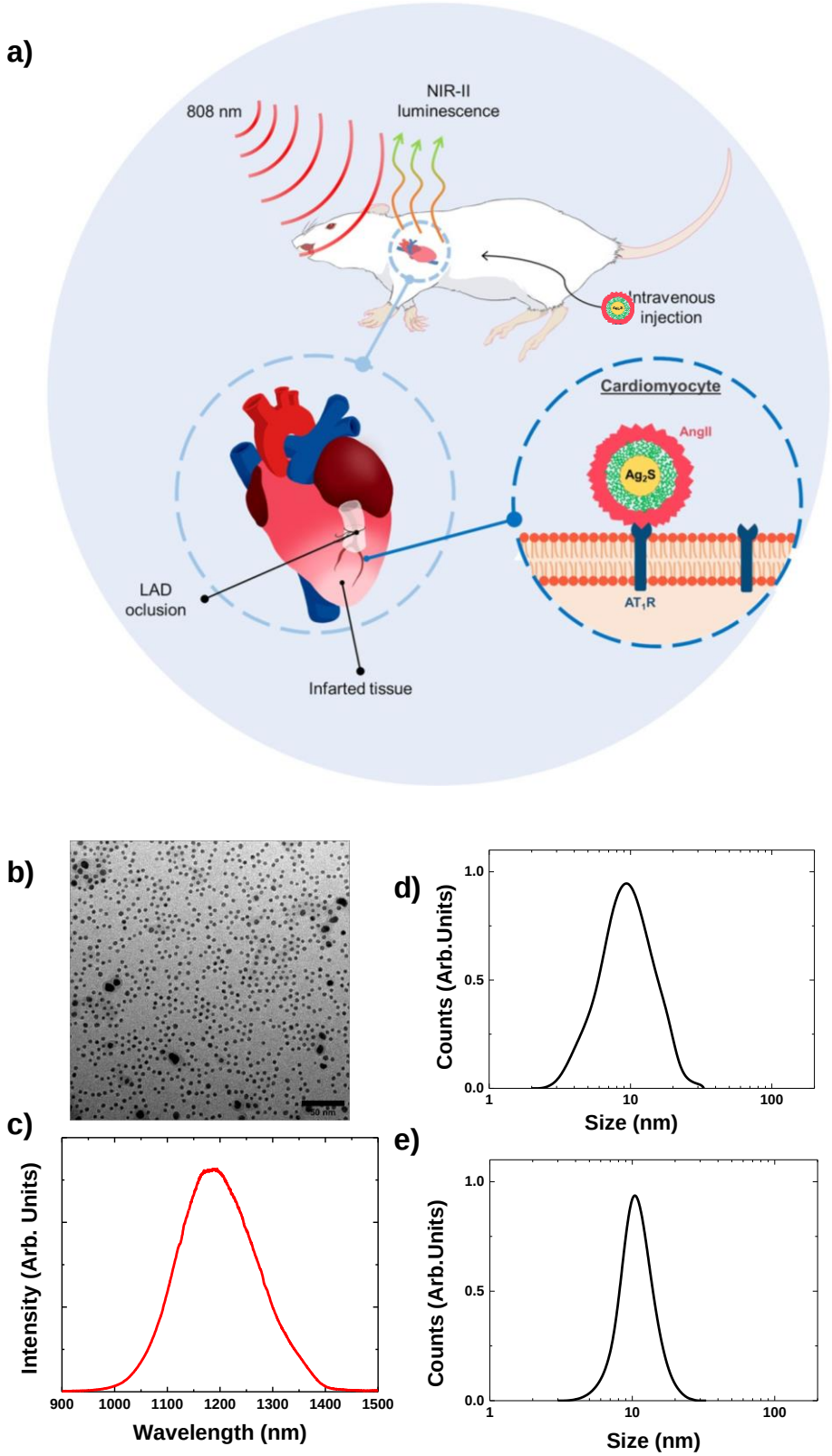

Figure 1. (a) Schematic representation of the experimental procedure followed in this work for *in vivo* imaging of acute infarct. **(b)** TEM image of Ag_2S dots used in this work. Scale bar: 50 nm **(c)** Emission spectra obtained from a colloidal suspension of Ag_2S dots as obtained under 790 nm optical excitation. **(d)** and **(e)** DLS graphs of AngII-functionalized and PEGylated Ag_2S NDs, respectively. In both cases a hydrodynamic radius close to 10 nm is obtained.

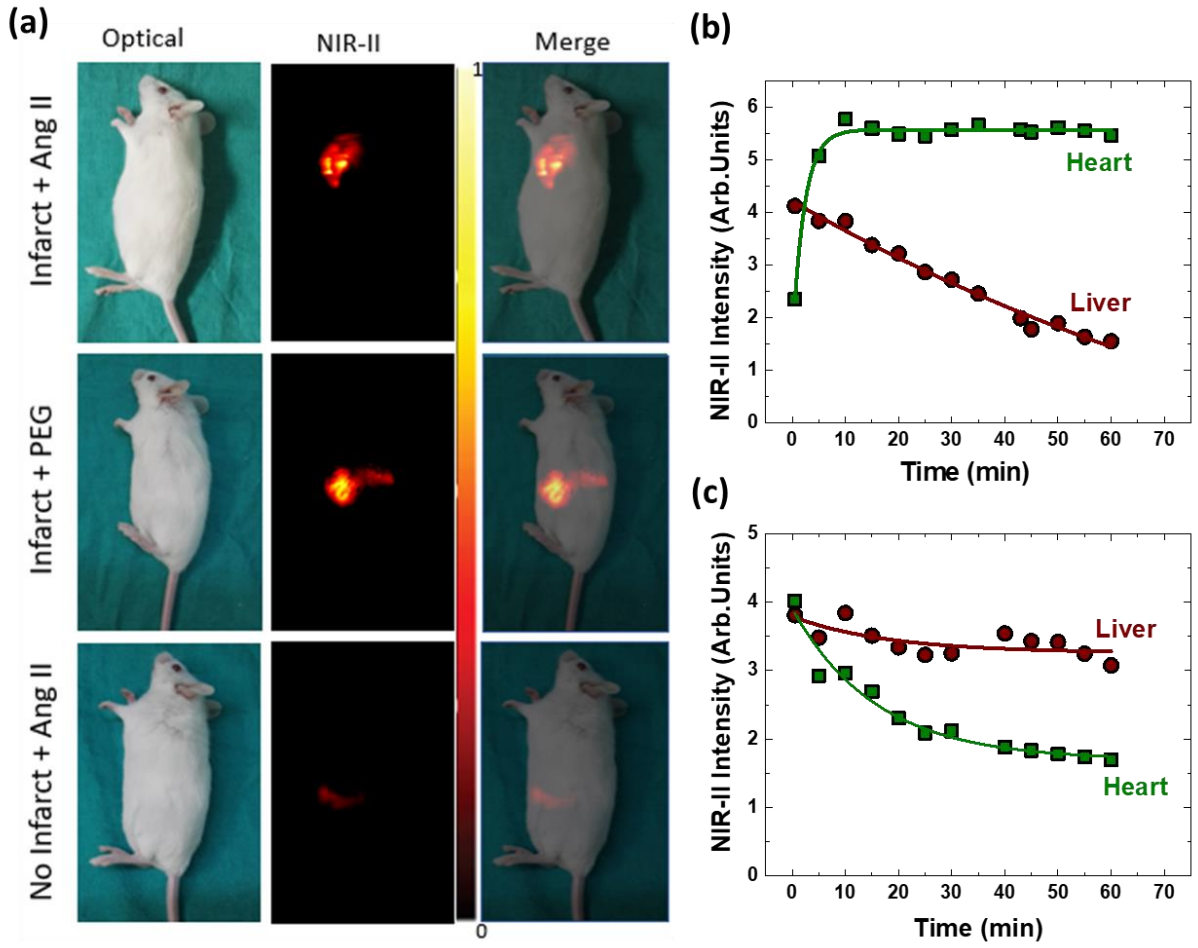

Figure 2. (a) Optical, NIR-II fluorescence and merge images of three representative mice corresponding to the three scenarios presented. Top row corresponds to a mouse subjected to an acute infarct followed by an intravenous injection of AngII-functionalized Ag_2S dots. Middle row corresponds to a mouse subjected to an acute infarct followed by an intravenous injection of PEGylated Ag_2S dots. Finally, the bottom row corresponds to a healthy mouse (without any infarct) subjected to an intravenous injection of AngII-functionalized Ag_2S dots. **(b)** Time course of the NIR-II luminescence intensity generated at the heart and liver of a mouse subjected to an acute infarct and to an intravenous injection of AngII-functionalized Ag_2S dots. **(c)** Time course of the NIR-II luminescence intensity generated at the heart and liver of a mouse subjected to an acute infarct and to an intravenous injection of PEGylated Ag_2S dots. In (b) and (c) dots are experimental data and solid lines are guide for the eyes.

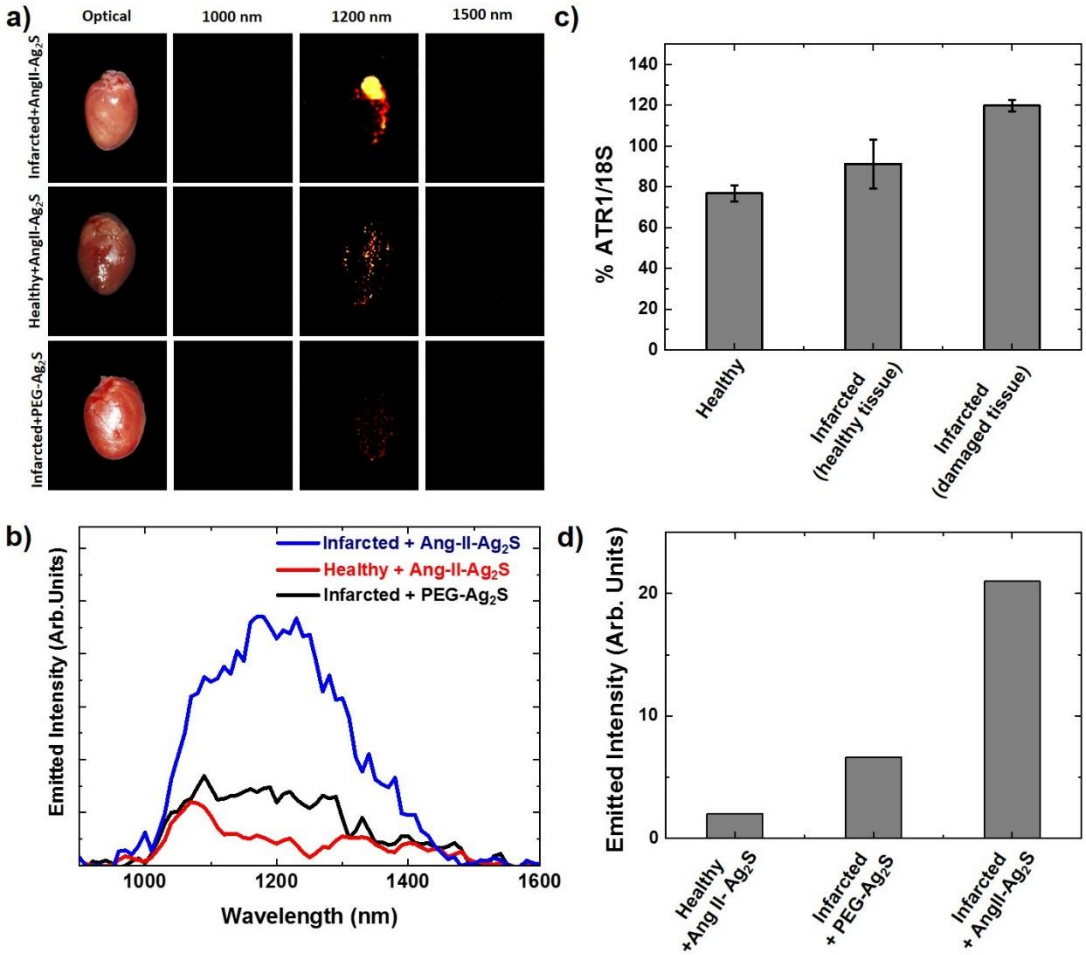

Figure 3. (a) *Ex vivo* fluorescence images at three different emission wavelengths (1000, 1200 and 1500 nm) as obtained for a heart subjected to an acute infarct and an intravenous injection of AngII-functionalized Ag_2S NDs, a healthy heart subjected to an intravenous injection of AngII-functionalized Ag_2S NDs and of a heart subjected to an acute infarct and intravenous injection of PEGylated Ag_2S NDs. The emission spectra corresponding to each case are shown in **(b)**. **(c)** mRNA levels of AT-1 in myocardial tissue from sham operated-mice and mice subjected to myocardial infarction. **(d)** Emitted intensity in the 1000-1600 nm range by a healthy and infarcted heart after intravenous injection with AngII-functionalized Ag_2S NDs and for an infarcted heart after intravenous injection with PEGylated Ag_2S NDs.

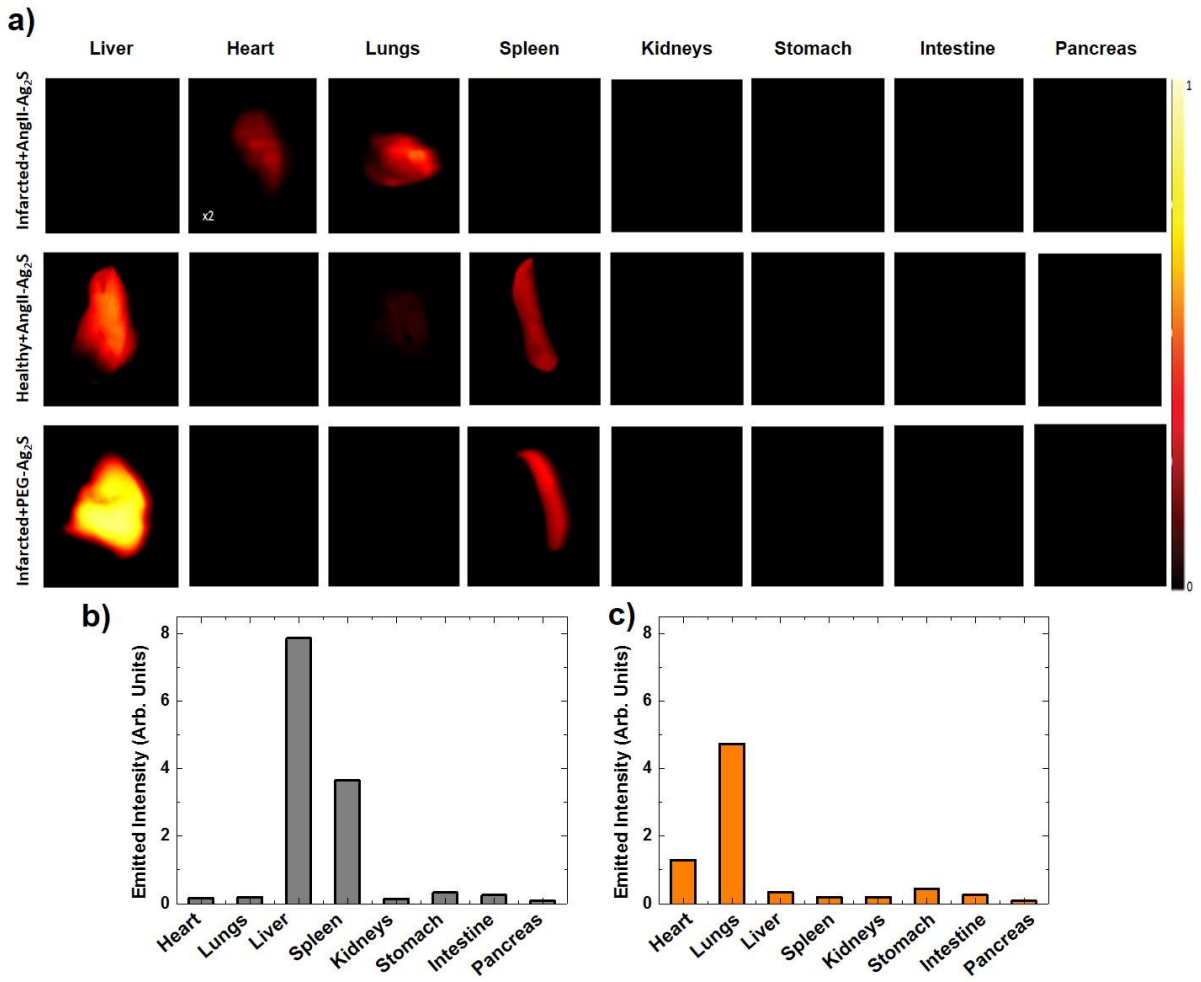

Figure 4. (a) *Ex vivo* NIR-II fluorescence images of the dissected organs corresponding to a healthy and infarcted mouse after intravenous injection of AngII-functionalized Ag_2S NDs and to a mouse subjected to an acute infarct and subsequent intravenous injection with PEGylated Ag_2S dots. Intensity histograms of the luminescence generated by the Ag_2S NDs accumulated in the different organs as obtained for a mouse subjected to an acute infarct and to a subsequent intravenous injection with PEGylated Ag_2S NDs (**(b)**) and with AngII-functionalized Ag_2S NDs (**(c)**).

Table 1. In vivo NIR fluorescence imaging of myocardial infarction with luminescent nanoparticles. Previous works were able to visualize damage 4 days after permanent infarction and 2 days after reversible ligation / reperfusion employing NIR-I imaging close to the visible. This works allows direct near real-time imaging of acute infarction 30 min post reperfusion and less than 10 min after injection of Ag_2S NDs.

Nanoparticle system	λexc [nm]	λem [nm]	Functionalization	Type of myocardial infarct	Time to imaging post infarct / post injection	Ref.
Clio-Cy5.5	672	680-720	Dextran/Cy 5.5	Permanent ligation	96 h / 48 h	[47]
CLIO-VT750	750	780	Dextran protease substrates	Permanent ligation / reperfusion	96 h / 24 h	[48]
Prosense680	680	700			48 h / 24 h (reperfusion)	
Ag_2S-AngII	808	1200	PEG-AngII	Reperfusion	30 min / 5 min	This work

The table of contents entry should be 50–60 words long and should be written in the present tense and impersonal style (i.e., avoid we). The text should be different from the abstract text.

Keyword NIR-II bioimaging

S. Mateos, C. Li, T. Muñoz-Ortiz, M. de la Fuente, J. Lifante, A. L. Villalon, M. Granada, J. Rubio Retama, D. Jaque, D. H. Ortgies*, N. Fenrández* ((same order as byline))

Instantaneous NIR-II *in vivo* imaging of acute myocardial infarct by NIR-II luminescent nanodots

ToC figure ((Please choose one size: 55 mm broad × 50 mm high **or** 110 mm broad × 20 mm high. Please do not use any other dimensions))

Supporting Information

Fast NIR-II *in vivo* imaging of acute myocardial infarct by NIR-II luminescent nanodots

Sergio Mateos, Chunyan Li, Tamara Muñoz-Ortiz, María de la Fuente, José Lifante, Angel Luis Villalon, Miriam Granado, Jorge Rubio Retama, Daniel Jaque, Dirk H. Ortgies and Nuria Fernández**

S1 Additional TEM micrograph of PEGylated Ag_2S nanodots

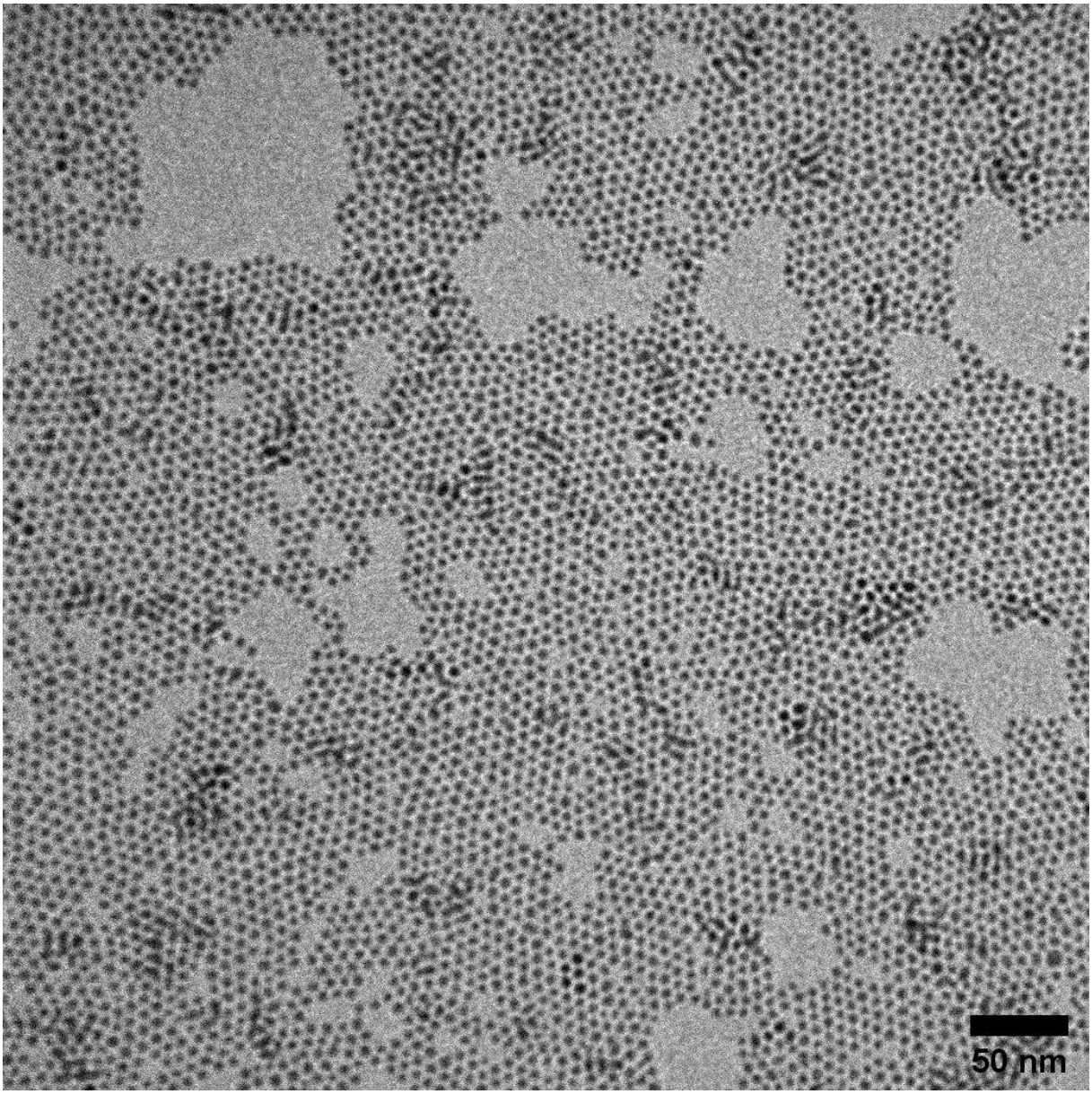

Figure S1. TEM Micrograph of PEGylated Ag_2S NDs

S2 FTIR characterization of Ag_2S nanodots

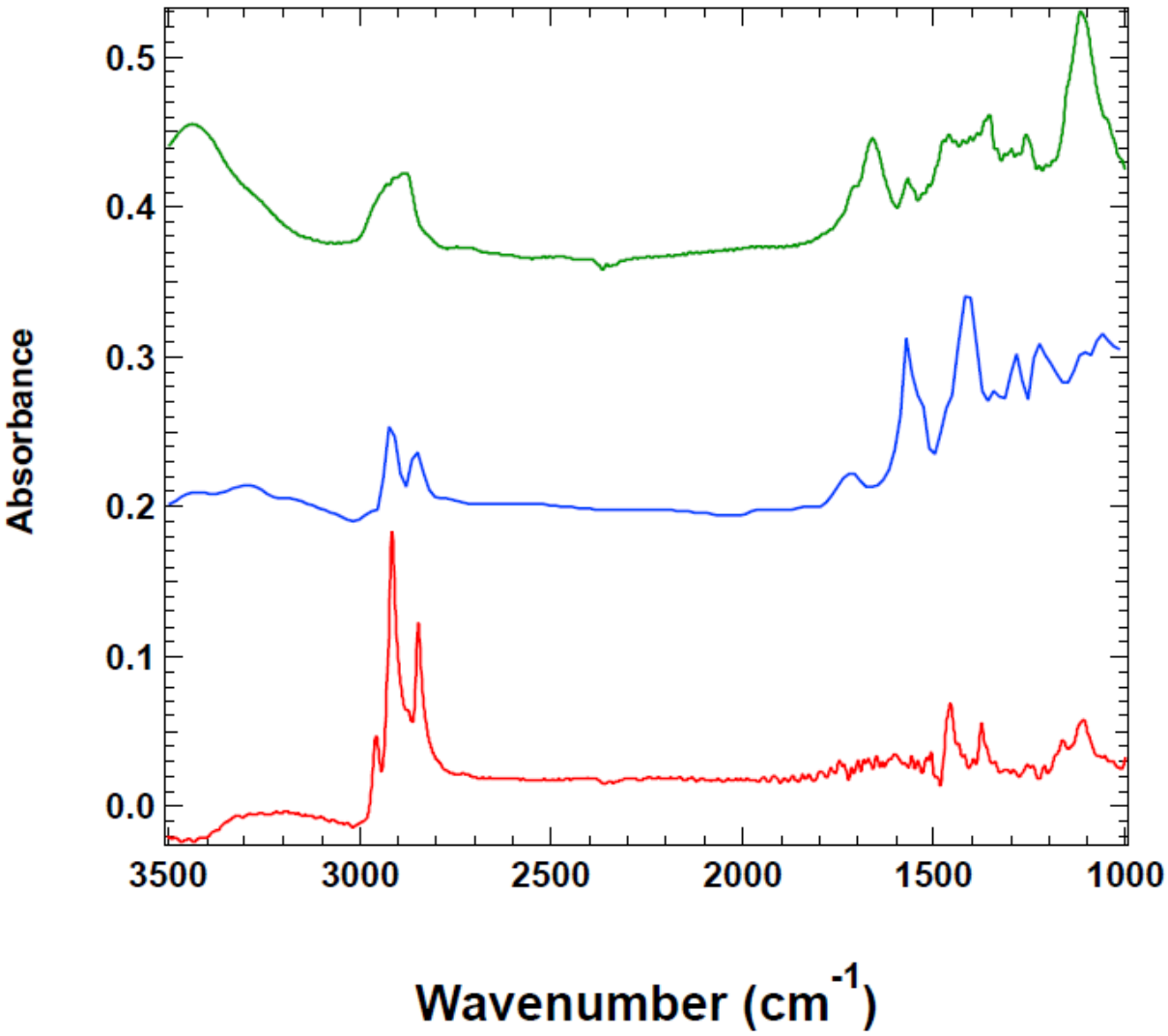

Figure S2. FTIR spectra of Ag_2S NDs with different surface functionalities; dodecanethiol capped Ag_2S NPs in red, 11-mercaptoundecylcarboxylic acid capped Ag2S NPs in blue and PEG (MW=2500 g/mol) functionalized Ag_2S NDs in green. All the spectra were acquired in a Nicolet IR200 FTIR spectrometer.

S3. Triphenyl Tetrazolium Chloride (TTC) staining for infarction assessment

The myocardial infarct size was determined by a TTC staining of the explanted hearts. The hearts were kept frozen at -80 ºC prior to the staining. The heart was cut into slices of 1 mm and incubated with TTC 1% during 20 min at 37 ºC, after that the slices were placed in phosphate buffered saline (PBS) overnight, which increased the contrast between the infarct area and the healthy area, thus obtaining a better visualization of the tissue. TTC precipitates with red colour if the tissue is non-affected by the infarct because mitochondria dehydrogenases are active and can perform the reaction with the dye, while dead tissue

remains pale. (Redfors B, Shao Y, Omerovic E. Myocardial infarct size and area at risk assessment in mice. Experimental and clinical cardiology 2012;17(4):268.)

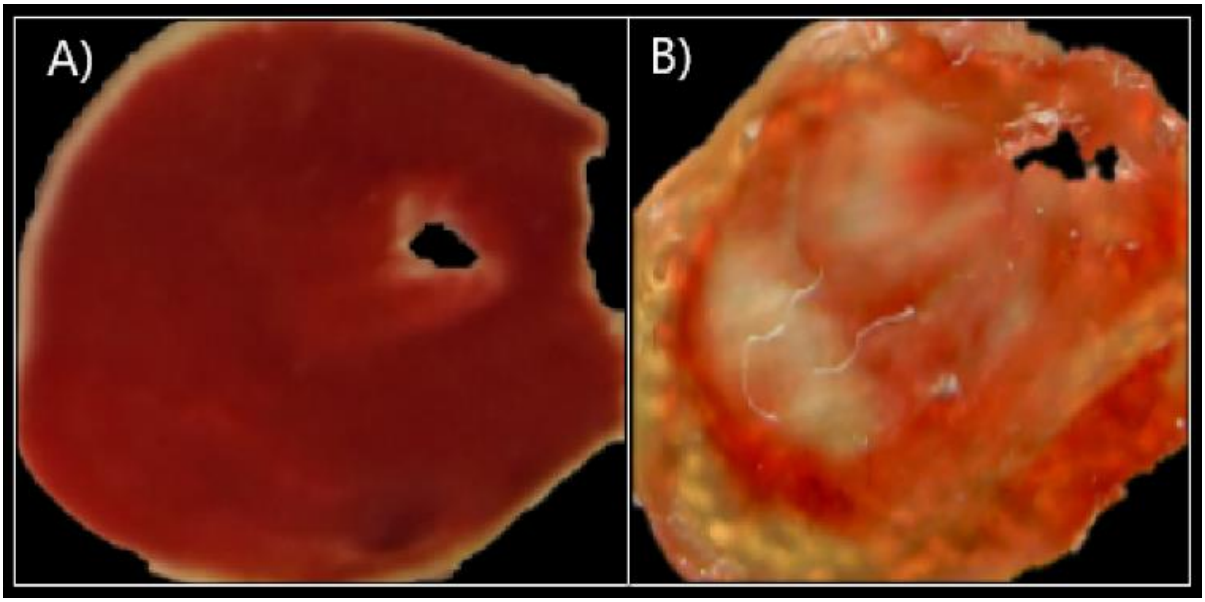

Figure S3. (a) A control heart (sham operation) that shows only healthy tissue and no damaged tissues after TTC staining (b) In the cut obtained from an infarcted heart the damaged tissues are identified after staining pale areas, while healthy tissues stay red.